Thieme

Tapirira guianensis is Selectively Cytotoxic, Induces Apoptosis to the Glioblastoma and Decreases Tumor Growth and Angiogenesis *in vivo*

Authors

Ana Gabriela Silva Oliveira[1], Marina Andrade Rocha[1], Lucas Santos de Azevedo[1], Aline Thaynara de Moura Coelho[1], Rafael César Russo Chagas[1], Hélio Batista Santos[2], Ralph Gruppi Thomé[2], Peter Samuel[3], Evelyn Wolfram[3], Bonglee Kim[4], Rui Manuel Reis[5,6], Rosy Iara Maciel Azambuja Ribeiro[1]

Affiliations

1 Experimental Pathology Laboratory, Midwest Campus, Federal University of São João del-Rei, Divinópolis, Brazil
2 Tissue Processing Laboratory, Midwest Campus, Federal University of São João del-Rei, Divinópolis, Brazil
3 Zurich University of Applied Sciences, Department of Life Sciences and Facility Management, Wädenswil, Switzerland
4 Department of Pathology, College of Korean Medicine, Kyung Hee University, Seoul, Republic of Korea
5 Molecular Oncology Research Center, Barretos Cancer Hospital, Barretos, Brazil
6 Life and Health Sciences Research Institute (ICVS), School of Medicine, University of Minho, Portugal

Key words

Glioblastoma, cerrado, *Tapirira guianensis*, Anacardiaceae, apoptosis, angiogenesis

received	April 5, 2023
accepted after revision	September 19, 2023
published online	October 13, 2023

Bibliography

Planta Med 2024; 90: 13–24
DOI 10.1055/a-2181-2569
ISSN 0032-0943

Georg Thieme Verlag KG, Rüdigerstraße 14, 70469 Stuttgart, Germany

Correspondence

Prof. Iara Maciel de Azambuja Ribeiro PhD
Experimental Pathology Laboratory (Sala 209, bloco E), Midwest Campus, Federal University of São João del-Rei
Rua Sebastião Gonçalves Coelho 400, 35501-296 Chanadour – Divinópolis-MG, Brazil
Phone: + 55 37 91 61 91 55, Fax: + 55 37 36 90 44 89
rosy@ufsj.edu.br

Supplementary material is available under https://doi.org/10.1055/a-2181-2569

ABSTRACT

Glioblastoma is the most frequent primary malignant brain tumor without effective treatment, which makes this work extremely relevant. The study of the bioactive compounds from medicinal plants plays an important role in the discovery of new drugs.

This research investigated the constituents of *Tapirira guianensis* and its antitumor potential (*in vitro* and *in vivo)* in glioblastoma. The *T. guianensis* extracts were characterized by mass spectrometry. The ethyl acetate partition (01ID) and its fractions 01ID-F2 and 01ID-F4 from *T. guianensis* showed potential antitumor treatment evidenced by selective cytotoxicity for GAMG with IC50 14.1 µg/mL, 83.07 µg/mL, 59.27 µg/mL and U251 with IC50 25.92 µg/mL, 37.3 µg/mL and 18.84 µg/mL. Fractions 01ID-F2 and 01ID-F4 were 10 times more selective when compared to TMZ and 01ID for the two evaluated cell lines. *T. guianensis* also reduced matrix metalloproteinases 2–01ID-F2 (21.84%), 01ID-F4 (29.6%) and 9–01ID-F4 (73.42%), ID-F4 (53.84%) activities, and induced apoptosis mainly through the extrinsic pathway. Furthermore, all treatments significantly reduced tumor size (01ID $p < 0,01$, 01ID-F2 $p < 0,01$ and 01ID-F4 $p < 0,0001$) and caused blood vessels to shrink *in vivo*. The present findings highlight that *T. guianensis* exhibits considerable antitumor potential in preclinical studies of glioblastoma. This ability may be related to the phenolic compounds and sesquiterpene derivatives identified in the extracts. This study deserves further *in vivo* research, followed by clinical investigation.

Introduction

Glioblastoma (GBM) is one of the most hostile malignant neoplasms that affect the central nervous system, classified as grade IV, and originates from astrocytic glial cells or their precursors [1]. The incidence of glioblastoma ranges from 3.19 to 4.17 cases per 100 000 person-years [2]. This tumor manipulates the microenvironment around it, supporting and stimulating angiogenesis, in addition to suppressing the immune system [3].

The current treatment for glioblastoma is surgical resection, followed by radiotherapy and chemotherapy with temozolomide, but these treatments have a low impact on median survival, which remains only 15 months [1–4]. Therefore, the attempt to achieve a cure for glioblastoma is still fruitless. Factors such as the blood vascularized network, the nonselective effect of TMZ, in addition to the blood–brain barrier, can lead to chemotherapy resistance, myelosuppression and difficulty in delivering drugs to tumor cells [5]. The inhibitory effects of natural products on angiogenesis and metastasis are encouraging. These effects also include the induction and acceleration of apoptosis and the production of reactive oxygen species, which have anti-metastasis effects. In addition, these effects may be combined with the reductions in toxicity and side effects [6].

Between 1981 and 2014, the Food and Drug Administration approved more than 1500 drugs, of which 38% were obtained or based on natural products [7]. Regarding antitumor drugs, 35% of these originate directly or indirectly from natural products, of which approximately 25% originate from plants [8]. We previously reported the cytotoxic activity of the ethyl acetate partition of *Tapirira guianensis* and its ability to inhibit tumor migration and invasion in oral cancer cell lines [9]. This plant also inhibited MMP-2 activity [10]. Herein, we investigated the antitumor activity of this specie in glioblastoma cell lines both *in vitro* and *in vivo*.

Results and Discussion

Temozolomide (TMZ) is the only effective chemotherapy in glioblastoma treatment [11]. However, the response is limited, with an average survival time of only 16 months, which changed little over the past decade [12]. These reactions can occur because of the low selectivity of TMZ for tumor cells, as demonstrated in another study by our group [13]. So, a desirable resource in the search for new therapies is the selectivity of treatment.

Among the evaluated *Tapirira guianensis* partitions, 01ID exhibited IC50 of 14.1, 25.92 and 24.88 µg/mL for GAMG, U251 and NHA cell lines, respectively. These values were lower than those found for temozolomide (▶ **Table 1**). Regarding the selectivity index (SI), it was observed that the ethyl acetate partition is as selective as its fractions (▶ **Table 2**). Fractions 01ID-F2 and 01ID-F4 were 10 times more selective when compared to both TMZ and 01ID for the two cell lines evaluated. The ideal drug should have a relatively high toxic concentration but with a very low active concentration [14]. Regarding cellular characteristics, we observed that cancer cells could migrate and form a tumor mass, which is not observed in normal cell lines, which are differentiated. In addition, the GAMG and U251 lineages have the TP53 and TERT records, and the U251 still has the CDKN2A/B and PTEN records [15,16,42,43]]. Meanwhile, the NHA does not present cells, being of normal cerebral tissue origin [15, 16].

▶ **Table 1** The IC50 values of exposure to 01ID partition, fractions 01ID-F2 and 01ID-F4 of *T. guianensis* and TMZ in GAMG, U251 and NHA cells at 72 hours.

Cell lines	01ID	01ID-F2	01ID-F4	TMZ
GAMG	14.1 ± 1.14	13.18 ± 1.12	22.34 ± 1.34	75.58 ± 1.87
U251	25.92 ± 1.41	4.83 ± 0.68	6.72 ± 0.82	167.3 ± 2.22
NHA	24.88 ± 1.39	130.3 ± 2.11	405 ± 2.6	48.49 ± 1.69

▶ **Table 2** Tumor selectivity index after treatment with partition 01ID and fractions 01ID-F2 and 01ID-F4 and chemotherapy TMZ for 72 hours.

Cell line	01ID	01ID-F2	01ID-F4	TMZ
GAMG	1.76	9.89	18.13	0.64
U251	0.96	26.95	60.28	0.29

Extracts derived from *T. guianensis* leaves showed high selectivity for tumor cells, making them relevant as possible chemotherapeutic agents for this neoplasm treatment. These results agree with our previous study, in which the ethyl acetate extract of *T. guianensis* decreased the cell viability of head and neck tumor cell lines [9]. Here, we also demonstrate that the fractions 01ID-F2 and 01ID-F4, derived from this extract, have a purer constitution and, in addition to their cytotoxicity, were 10 times more selective.

Another characteristic of glioblastoma is its high ability to proliferate and invade adjacent tissues fast [17, 18]. Only the ethyl acetate partition inhibited the glioblastoma cells' migration. These can indicate that the separation process in the fractionation may have lost the compounds with this capacity or that compounds that act synergistically present in the partition have been separated and, thus, lost the activity [19, 20]. The 01ID significantly reduced cell migration of GAMG and U251 glioblastoma cells at 24, 48 and 72 hours; $p < 0.05$, $p < 0.01$ (▶ **Fig. 1 a**). However, no significant capability to reduce cell migration was observed (▶ **Fig. 1 b**).

Condensation and fragmentation of nuclear material and apoptotic bodies were observed in the cells GAMG and U251 after exposure to the partition and fractions (Fig ▶ **2**). Exposure to the *T. guianensis* partition and fractions decreased the activity of metalloproteinases 2 and 9. Exposure to 01ID caused an additional decrease in MMP-9 activity by 76.00% ± 11.71 ($p = 0.0142$) (▶ **Fig. 3 a, b**) regarding the effect on MMP-2 (33.31% ± 6.05 ($p = 0.0161$)) (▶ **Fig. 3 e, f**). Fractions 01ID-F2 and 01ID-F4 were also more effective in decreasing MMP-9 activity 73.43% ± 0.97 ($p < 0.0001$) and 53.84% ± 1.55 ($p = 0.0004$) (▶ **Fig. 3 c, d**), respectively. For MMP-2, the action of fractions 01ID-F2 and 01ID-F4 caused a decrease of 21.84% ± 2.14 ($p < 0.0001$) and 29.60% ± 2.46 ($p < 0.0034$), respectively (▶ **Fig. 3 g, h**).

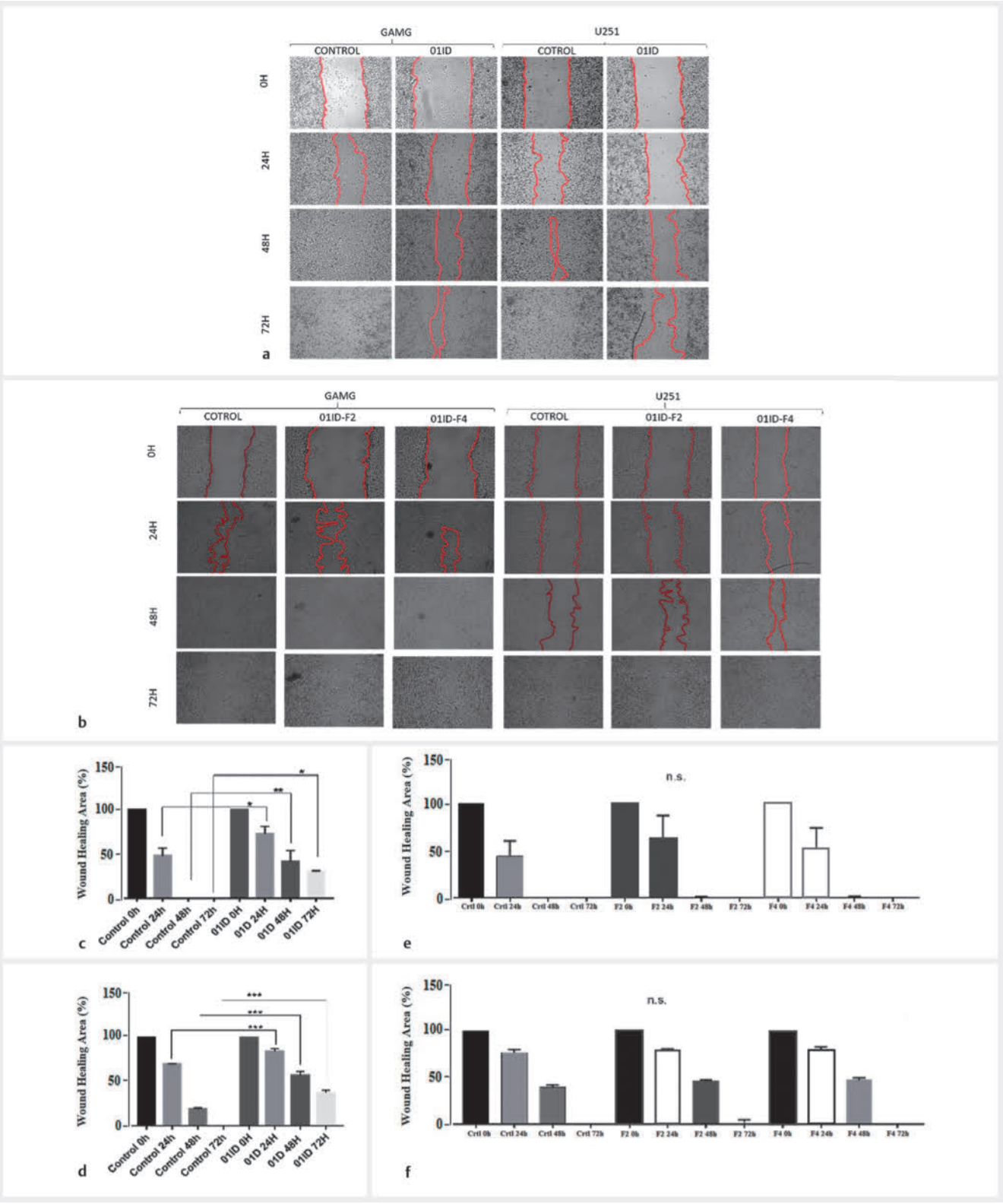

▶ **Fig. 1** Cell migration of GAMG and U251 cell lines after treatment with the 01ID and its fractions of *T. guianensis*. **a** Representative images at times 0, 24, 48 and 72 hours with treatment 01ID. **b** Representative images at times 0, 24, 48 and 72 hours with treatment 01ID-F2 and 01ID-F4. **c** Graphs of the wound area in the GAMG strain at times 0, 24, 48 and 72 hours with the treatment 01ID. **d** Graphs of wound area in the U251 strain at times 0, 24, 48 and 72 hours with the treatment 01ID. **e** Graphs of the wound area in the GAMG strain at times 0, 24, 48 and 72 hours with the treatment 01ID-F2 and 01ID-F4. **f** Graphs of wound area in the U251 strain at times 0, 24, 48 and 72 hours with the treatment 01ID-F2 and 01ID-F4. Data are represented as mean and standard deviation. Statistical analysis by Tukey's multiple comparisons test. * $p < 0.05$, ** $p < 0.01$, *** $p < 0.001$, n. s.: no significance.

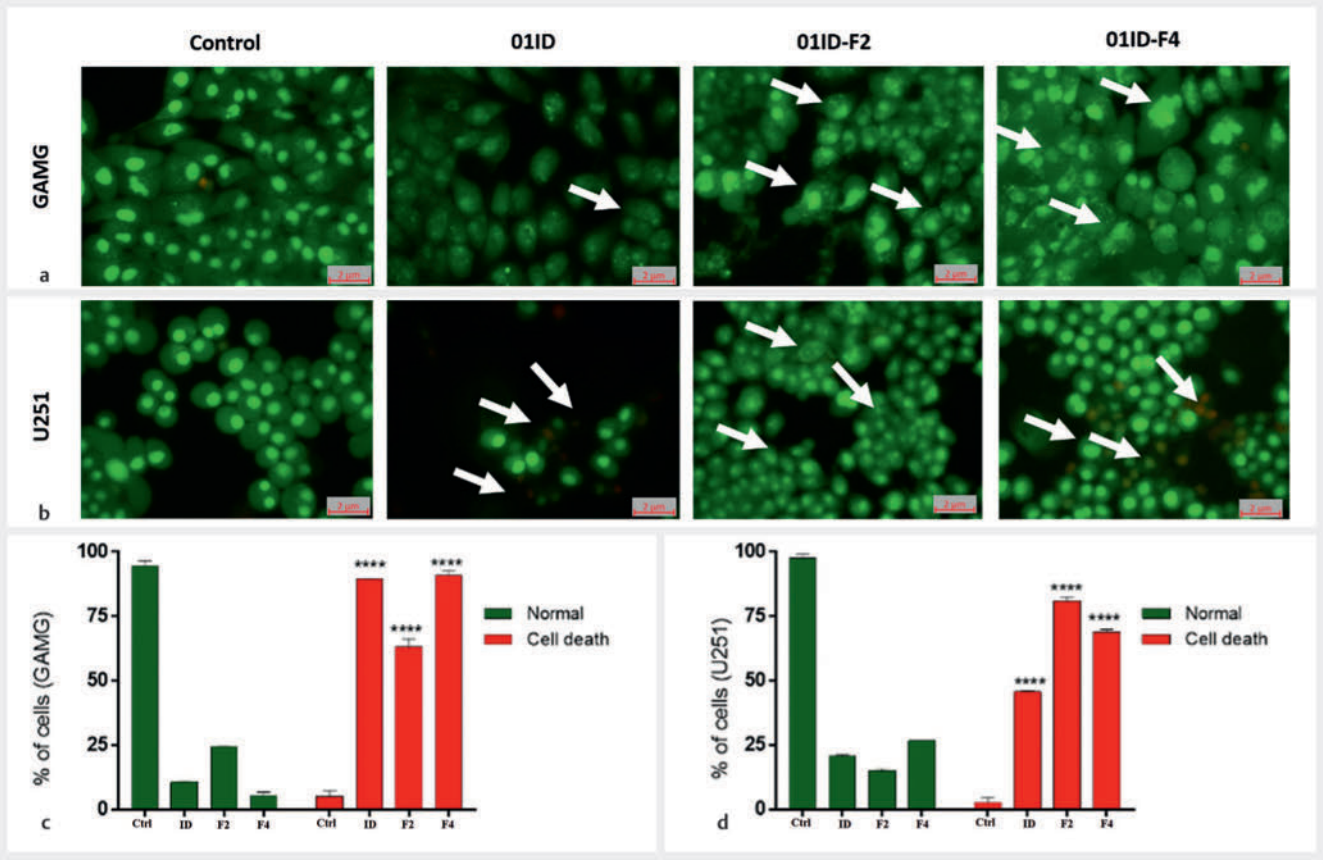

▶ **Fig. 2** Fluorescence morphological assay using AO/PI double staining in GAMG and U251 cell lines after exposure with the 01ID and its fractions. **a** Representative images of control and fractions in the GAMG. **b** Representative images of control and treatments in the U251. **c** and **d** Graphs of viable and dying cell numbers in the GAMG and U251 tumor lines, respectively. Data are represented as mean and standard deviation. Statistical analysis by *t*-test, **** $p < 0.0001$.

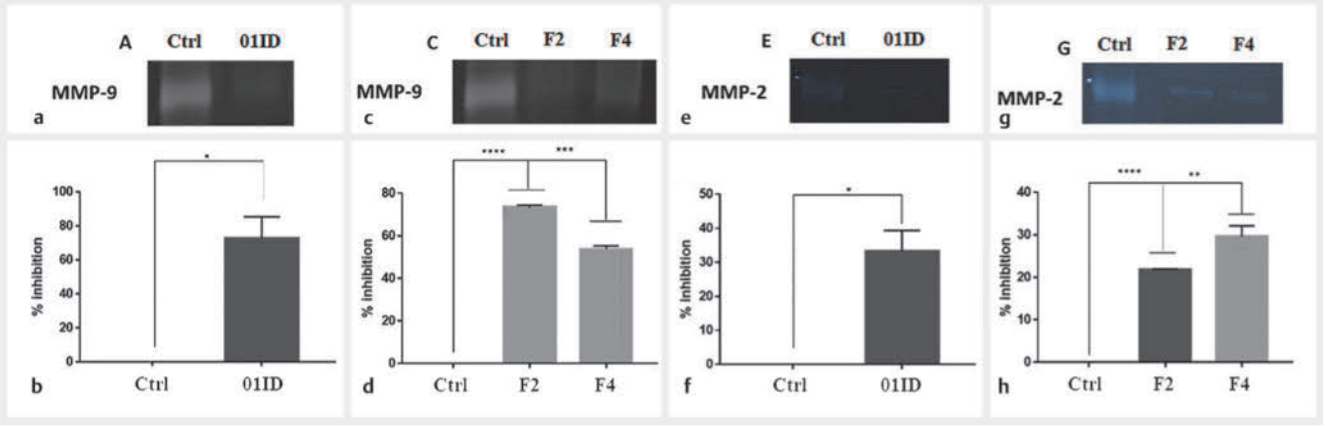

▶ **Fig. 3** Zymography after treatment with the 01ID partition of *T. guianensis*. Zymographic images of the action of *T. guianensis* partition on MMP-9 (**a**) and MMP-2 (**e**) and graphs representing the percentage of this inhibition of activity in MMP-9 (**b**) and MMP-2 (f). Zymography images representing the action of fractions (01ID-F2 and 01ID-F4) of *T. guianensis* on MMP-9 (**c**) and MMP-2 (**g**) and the graphs representing the percentage of this inhibition in MMP-9 (**d**) and MMP-2 (**h**). Data are represented as mean and standard deviation. Statistical analysis by *t*-test, * $p < 0.05$, ** $p < 0.0034$, *** $p = 0.0004$, **** $p < 0.0001$ compared to untreated control.

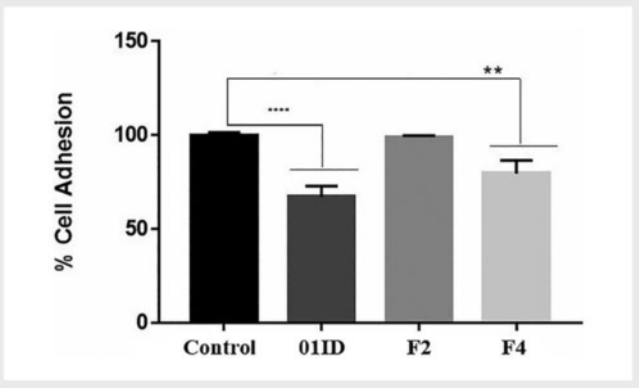

▶ **Fig. 4** Cell adhesion assay after exposure with the ethyl acetate partition of *T. guianensis*. Graph of percentage inhibition of cell adhesion. Data are represented as mean and standard deviation. Statistical analysis by *t*-test, ** $p < 0.0013$, **** $p < 0.0001$.

The 01ID reduced by 32.81% ± 5.79 ($p < 0.0001$) the cell adhesion (▶ **Fig. 4**). There was no reduction in adherence after treatment with fraction 01ID-F2. However, fraction 01I-F4 showed a significant decrease in cell adhesion of 20.38 ± 6.98 cell adhesion ($p < 0.0013$) (▶ **Fig. 4**).

There was a significant increase in proteins related to the apoptotic death pathway when cells were treated with the compounds. An increase in TNF-R1 was observed in 52.5% ($p < 0.001$), 88.19% ($p < 0.01$) and 91.86% ($p < 0.001$) when cells were treated with fractions 01ID, 01ID-F2 and 01ID-F4, respectively. FAAD expression increased significantly by 37.93% ($p < 0.001$), 57.96% ($p < 0.05$) and 51.20% ($p < 0.01$) for treatments 01ID, 01ID-F2 and 01ID -F4, respectively. We also observed a significant increase in caspases 8, 7 and 3. Caspase 8 increased 72.41% ($p < 0.001$), 71.92% ($p < 0.001$) and 87.74% ($p < 0.001$) for treatments 01ID, 01ID-F2 and 01ID-F4, respectively. Caspase 7 also showed significant increases of 45.14% ($p < 0.01$), 71.92% ($p < 0.01$) and 77.74% ($p < 0.001$) for treatments 01ID, 01ID-F2 and 01ID-F4, respectively. Finally, there was an increase in caspase 3 of 72.91% ($p < 0.01$), 92.31% ($p < 0.01$) and 102.29% ($p < 0.0001$) (▶ **Fig. 5**).

The increased expression of TNF-R1, FADD, and caspases 8, 7 and 3 found in our study is related to cell death by extrinsic apoptosis [21]. This action can be attributed to compounds from the class of flavonoids found in *T. guianensis* samples, such as luteolin 7-O-glycoside and quercetin, previously associated with the induction of cell death by this cell death pathway [22]. Furthermore, studies in prostate and breast tumors showing that catechins, also present in *T. guianensis*, can induce cell death through this pathway [23, 24] support our results.

Cell proliferation and invasion are related to the activity of matrix metalloproteinases (MMPs) as they degrade extracellular matrix components, which helps in tumor progression and angiogenesis [15, 16]. The expression of metalloproteinases plays a vital role in the invasion of cancer cells in normal tissue, indirectly reducing the effectiveness of chemotherapy [25]. Therefore, inhibiting the expression of MMPs may be a remarkable strategy to control these processes [25]. In this study, we observed a reduc-

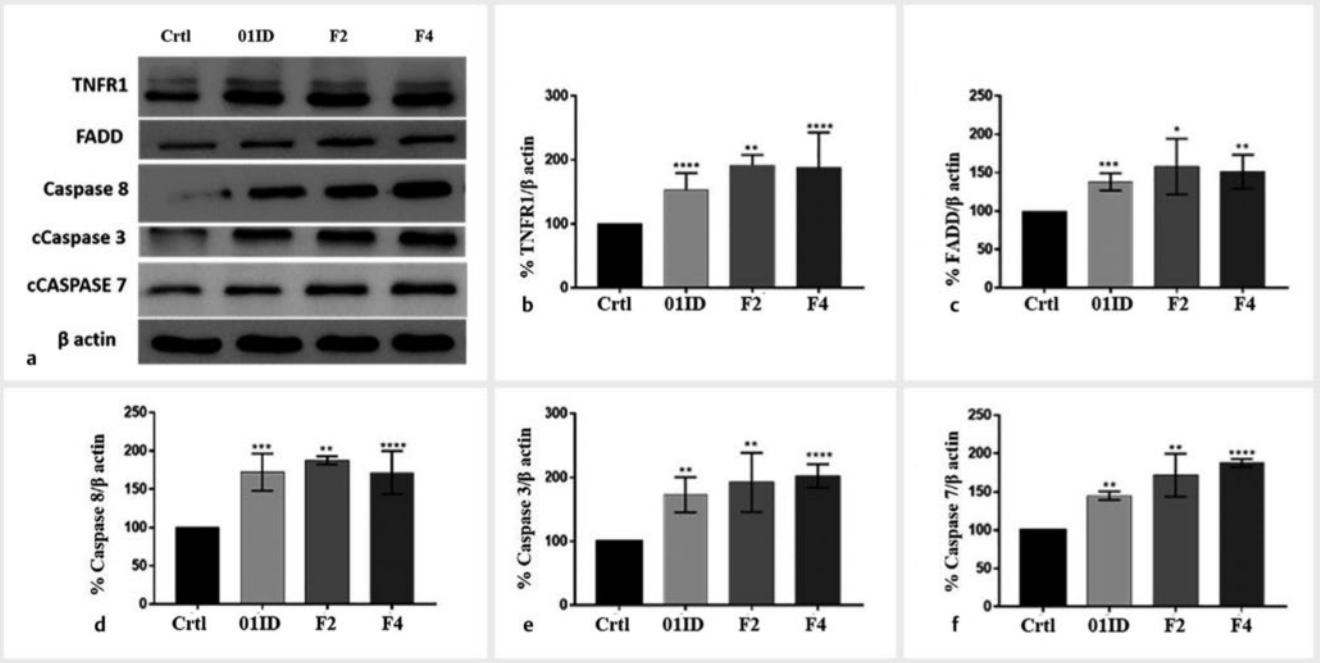

▶ **Fig. 5** Protein expression of apoptosis death pathway after treatment with ethyl acetate partition and its fractions. a Representative images of Western blotting. **b** Graph of percent protein expression of TNF-R1. (C) Graph of the percentage of protein expression of FADD. **d, e**, and **f** Graph of protein expression percentage of cleaved caspases 8, 7 and 3. Data are represented as mean and standard deviation. Statistical analysis by *t*-test. * $p < 0.05$, ** $p < 0.01$, *** $p < 0.001$.

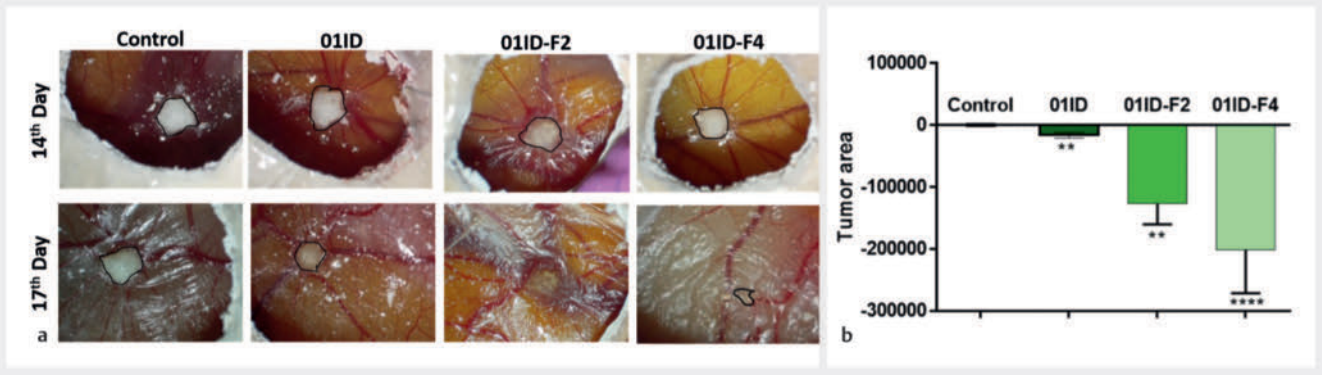

▶ **Fig. 6** Tumor perimeter, *in vivo*, in the chicken chorioallantoic membrane after treatment with *T. guianensis* extracts. **a** Representative images of the control group and the groups treated. **b** Graph of tumor perimeter. Statistical analysis by *t*-test, ** $p < 0.01$, **** $p < 0.0001$.

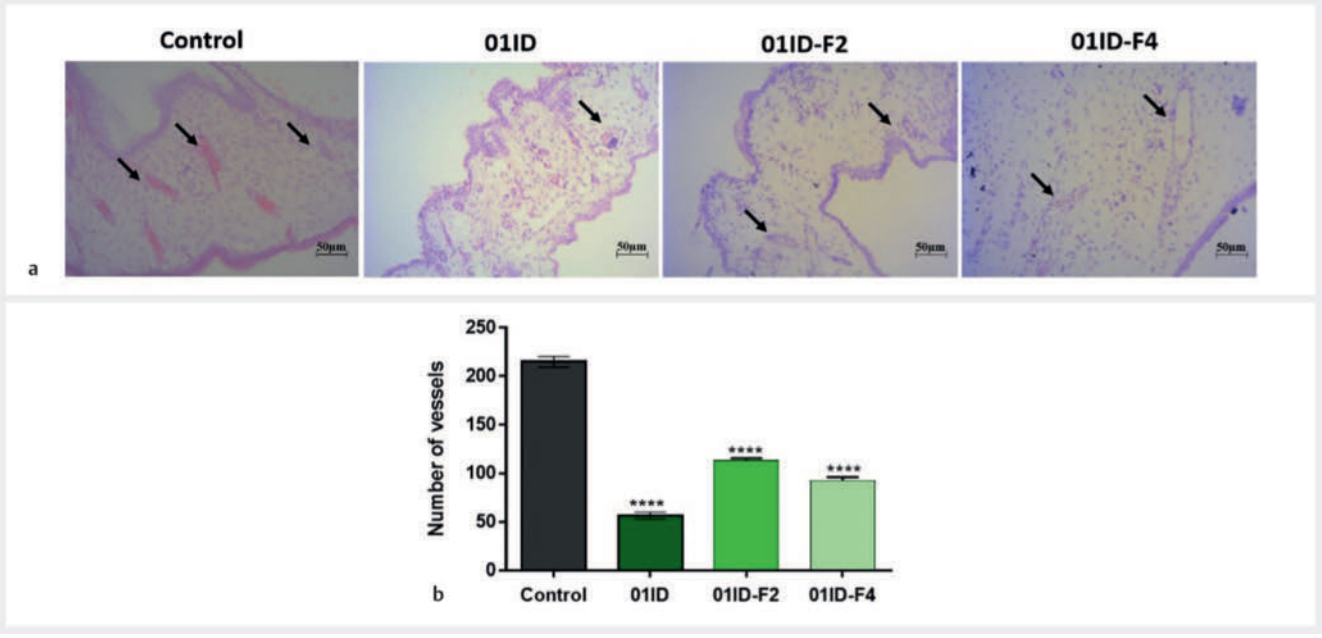

▶ **Fig. 7** Evaluation of angiogenesis in the chicken chorioallantoic membrane after treatment with 01ID partition. **a** Representative histological images of the control group and the groups treated. **b** Graph of the number of blood vessels. Statistical analysis by *t*-test, * $p < 0.0017$, **** $P < 0.0001$.

tion in the activity of MMPs 2 and 9, which may be related to the presence of quercetin in fractions 01ID and 01ID-F4. Studies have shown the potential of this flavonoid to inhibit MMP-2 in GL-15 glioblastoma cells and to inhibit MMP-2 and MMP-9 expressions in U251 [26, 27]. However, this inhibitory effect may also be related to the compound genistein, which only inhibits MMP-2 [28]. Another compound present in the extracts is catechin, which is related to the potential for inhibiting metalloproteinases (MMP-2 and 9) in several types of tumors, such as digestive, prostate and lung tumors [29].

Regarding the tumor perimeter reduction, 01ID, 01ID-F2 and 01ID-F4 were statistically significant ($p < 0.01$, $p < 0.01$ and $p < 0.0001$, respectively) (▶ **Fig. 6**). Moreover, CAMs were histologically analyzed to quantify the number of blood vessels in which significant reductions ($p < 0.0017$) were observed after treatment with the ethyl acetate partition extract and with the 01IDF-F2 and 01ID-F4 fractions (▶ **Fig. 7**). Furthermore, after exposure to *T. guianensis*, there was no effect on blood vessel lysis and bleeding (▶ **Fig. 8**).

One of the hallmarks of cancer is angiogenesis, which plays an essential role in tumor growth, invasion and metastasis. The chicken chorioallantoic membrane (CAM) model offers excellent advantages for both the macroscopic and microscopic study of tumor development to angiogenesis [30]. Because it is partially immunodeficient, the CAM can receive xenotransplants from other species without interfering with an immune reaction. The natural vascular network is another advantage, as it provides an interface that allows human tumors survival, growth and vascularization [31].

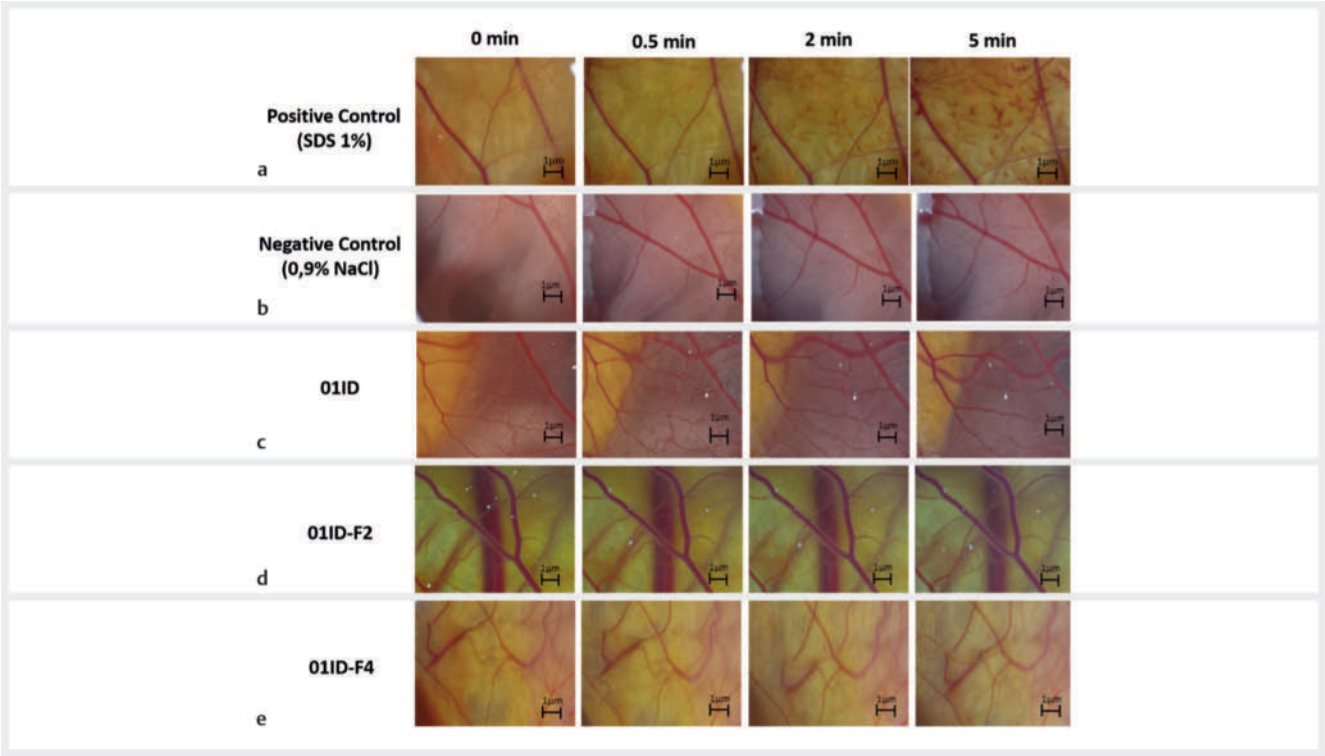

▶ **Fig. 8** The chorioallantoic membrane did not change after treatment with partition 01ID and its fractions 01ID-F2 and 01ID-F4 at 0.5 minutes, 2 minutes and 5 minutes. **a** Representative images after positive control treatment (1% SDS) with lysis and hemorrhage were observed at 2 and 5 minutes. **b** Representative images of the negative control (0.9% NaCl). **c, d**, and **e** Representative images of treatment with partitions 01ID, 01ID-F2 and 01ID-F4, respectively, at times 0, 0.5; 2 and 5 minutes, no change being observed.

The reduction in the perimeter of the tumor and angiogenesis found in our study may be related to the compounds present in the extracts, such as gallic acid, which has already been reported as an angiogenesis inhibitor in cervical tumors [32]. Catechins can also be related, as they were responsible for inhibiting tumorigenesis in several types of **tumors**, including glioblastoma, by inhibiting the apoptosis pathway and inhibiting proliferation, cell growth and angiogenesis [21–24, 28–34]. These substances, including epicatechin present in the 01ID-F4 fraction, may explain the best inhibition of **tumor** growth and corroborate the findings of Wang et al. (2019), who indicated that (−)-Epigallocatechin 3-O-gallate is a potent inhibitor of angiogenesis in an esophageal tumor [24].

The ethyl acetate extract (01ID) and the fractions 01ID-F2 and 01ID-F4 were analyzed by UPLC-QTOF/MS. Fifteen compounds were tentatively identified in 01ID: mainly phenolic compounds (▶ **Table 3**). In the 01ID-F2 fraction, 10 compounds were tentatively identified: mostly sesquiterpenes or fatty acids derivatives (▶ **Table 4**). In the 01ID-F4 fraction, 12 compounds were tentatively identified: mainly phenolic compounds (▶ **Table 5**).

Among the various routes of chemotherapy administration, the intravenous way is one of the most used in its administration. However, leakage of the venous network may occur, causing subcutaneous toxicity and causing damage to adjacent tissues, ulcerations and necrosis [35]. The HET-CAM, a variation of the CAM that was initially used to assess the risk of irritation of the skin and mucous membranes caused by exposure to new substances, also allows the measurement of the risk of irritancy of the infusion site, reducing the use of tests in mammals [36]. Thus, we also verified that the extracts of *Tapirira guianensis*, 01ID, 01ID-F2 and 01ID-F4, did not cause irritability, hemorrhage or blood clotting, suggesting that these samples can be administered parenterally [37].

The ethyl acetate partition from *T. guianensis* and its fractions are cytotoxic to glioblastoma tumor cells, the latter being more selective than partition. Also, they can induce cell death by extrinsic apoptotic pathways. Furthermore, partition and fractions effectively inhibited tumor growth and angiogenesis *in vivo*. This capacity may be due to compounds of the extracts such as the flavonoid class, such as the compounds luteolin 7-O-glucoside and quercetin or catechins. Ultimately, these findings may lead to new therapeutic strategies discovery against glioblastoma.

Materials and Methods

Obtaining extracts partition and fractions

Tapirira guianensis leaves were collected at latitude S18°58′08′′ and longitude W 49°27′54′′ by Allisson Rodrigues de Rezende, and the exsiccate was deposited in the Depositary Herbarium of the Federal University of Minas Gerais (143 407 BHCB), SISGEN Nº R6B8CA8. The leaves were dehydrated, pulverized and kept in a

▶ **Table 3** Qualitative analysis by UPLC-MS of 01ID fraction. Hi – Hibiscetin; Myr – Myricetin, Querc – Quercetin, (Epi)cat – (Epi)Catechin, Kaemp – Kaempferol, Hex – Hexosides, Pent-Pentosides

r_t (min)	Ions m/z	Formula	Error (ppm)	Tentative Identification	Detection Mode
0.697	191.0564	$C_7H_{12}O_6$	4.2	Quinic Acid	–
1.812	169.0143	$C_7H_6O_5$	3.6	Gallic Acid	–
2.54	495.0781	$C_{21}H_{20}O_{14}$	2.4	Hi-hex	–
2.557	495.0783	$C_{21}H_{20}O_{14}$	2.8	Hi-hex	–
3.026	479.0836	$C_{21}H_{20}O_{13}$	2.1	Myr-hex	–
	615.0995	$C_{28}H_{24}O_{16}$	1.5	Querc-galloyl-hex	
	729.1459	$C_{37}H_{30}O_{16}$	1.2	(Epi)cat-gallate dimer	
3.12	441.0837	$C_{22}H_{18}O_{10}$	4.8	(Epi)cat-gallate	–
	463.0894	$C_{21}H_{20}O_{12}$	3.7	Querc-hex	
	599.1056	$C_{28}H_{24}O_{15}$	3.2	Kaemp-galloyl-hex	
3.27	433.0783	$C_{20}H_{18}O_{11}$	2.8	Querc-pent	–
	441.0832	$C_{22}H_{18}O_{10}$	3.6	(Epi)cat-gallate	
	463.0892	$C_{21}H_{20}O_{12}$	3.2	Querc-hex	
	599.1056	$C_{28}H_{24}O_{15}$	3.2	Kaemp-galloyl-hex	
3.30	433.0781	$C_{22}H_{18}O_{11}$	2.3	Querc-pent	–
	447.0936	$C_{21}H_{20}O_{11}$	2.0	Kaemp-hex	
3.33	447.0938	$C_{21}H_{20}O_{11}$	2.5	Kaemp-hex	–
3.026	617.1131	$C_{28}H_{24}O_{16}$	− 1,9	Querc-galloyl-hex	+
3.125	303.0498	$C_{15}H_{10}O_7$	− 2,3	Quercetin	+
	465.1025	$C_{21}H_{20}O_{12}$	− 1,7	Querc-hex	
	601.118	$C_{28}H_{24}O_{15}$	− 2,2	Kaemp-galloyl-hex	
3.241	303.0493	$C_{15}H_{10}O_7$	− 4,0	Quercetin	+
	435.0914	$C_{20}H_{18}O_{11}$	− 3,0	Querc-pent	
	601.1174	$C_{28}H_{24}O_{15}$	− 3,2	Kaemp-galloyl-hex	
3.302	303.0495	$C_{15}H_{10}O_7$	− 3,3	Quercetin	+
4.538	318.2996	$C_{18}H_{39}NO_3$	− 2,2	4-hydroxysphinganine	+
4.968	302.3047	$C_{18}H_{39}NO_2$	− 2,3	Sphinganine	+
	346.3309	$C_{20}H_{43}NO_3$	− 2,0	Aminoeicosanetriol	

cool, dry, dark place. The powder was macerated in an alcoholic solution (70%) at a ratio of 1:5 and lyophilized to produce the crude extract (CE). The CE was suspended in an alcohol solution (70%) and fractionated by liquid–liquid extraction using hexane, chloroform and ethyl acetate in increasing order of their polarity. The ethyl acetate 01ID sample extract was collected, frozen and lyophilized. The fractions were obtained from the ethyl acetate partition, using columns (4 cm in diameter) for the fractionation. Silica gel 60 (230–400 Mesh-Sorbine Adsorbents Tecnologia Ltda.) was solubilized in the hexane/ethyl acetate (5:1) eluent and inserted into the column to a height of 15 cm with a silica pump vacuum (Prismatec). The fractions were collected every 10 mL. Thin-layer chromatography (CCD) evaluated fractions, and those with similar profiles were pooled and left six fractions at the end. Finally, the solvent of the fractions was removed using a rotary evaporator and desiccator, and the masses were measured in analytical balance (Mars).

From 6 g of crude extract, 0.633 g of ethyl acetate partition yield were obtained. From the 3.004 g mass of the partition, 0.045 g of fraction 01ID-F2 and 0.2026 g of fraction 01ID-F4 were obtained.

Cell culture

The commercial glioblastoma cell line used was GAMG (ACC 242) obtained from the German Collection of Microorganisms and Cell Cultures (DSMZ) and U251 (European Collection of Authenticated Cell Cultures (ECACC) Catalogue No. 09 063 001). In addition to the normal commercial NHA (Normal Human Astrocyte – CC-

▶ **Table 4** Qualitative analysis by UPLC-MS of 01ID-F2 fraction.

r_t (min)	Main Ions m/z	Formula	Error (ppm)	Tentative Identification	Detection Mode
3.512	187.098	$C_9H_{16}O_4$	2.2	Azelaic acid	–
4.924	293.1767	$C_{17}H_{26}O_4$	2.9	Gingerol	–
6.160	295.2287	$C_{18}H_{32}O$	2.8	Lineolic acid derivative	–
6.767	271.2285	$C_{16}H_{32}O_3$	2.3	Hexanedecanoic acid derivative	–
4.123	247.1321	$C_{15}H_{18}O_3$	− 2.8	Sesquiterpenes derivatives	+
4.233	237.1844	$C_{15}H_{24}O$	− 2.1	Sesquiterpenes derivatives	+
4.625	235.1694	$C_{15}H_{22}O_2$	0.4	Sesquiterpenes derivatives	+
4.774	217.1587	$C_{15}H_{20}O$	0.0	Sesquiterpenes derivatives	+
5.265	219.1741	$C_{15}H_{20}O_2$	− 0.9	Sesquiterpenes derivatives	+
5.585	359.2196	$C_{22}H_{30}O_4$	− 5.6	Palbinone	+

▶ **Table 5** Qualitative analysis by UPLC-MS of 01ID-F4 fraction.

r_t (min)	Ions m/z	Formula	Error (ppm)	Tentative Identification	Detection Mode
1.793	169.0144	$C_7H_6O_5$	0.9	Gallic Acid	–
2.471	153.0195	$C_7H_6O_4$	1.1	Dihydroxybenzoic acid	–
2.538	495.0781	$C_{21}H_{20}O_{14}$	2.4	Hi-hex	–
2.775	137.0244	$C_7H_6O_3$	− 0.1	Hydroxybenzoic acid	–
3.029	615.1002	$C_{28}H_{24}O_{16}$	2.6	Querc-galloyl-hex	–
3.122	463.0883	$C_{21}H_{20}O_{12}$	1.4	Querc-hex	–
	599.1049	$C_{28}H_{24}O_{15}$	2.0	Kaemp-galloyl-hex	
3.238	197.0461	$C_9H_{10}O_5$	2.8	Syringic acid	–
	417.0831	$C_{20}H_{18}O_{10}$	2.2	Kaemp-pent	
3.818	301.0359	$C_{15}H_{10}O_7$	3.7	Quercetin	–
4.127	285.0410	$C_{15}H_{10}O_6$	3.9	Kaempferol	–
3.026	617.1129	$C_{28}H_{24}O_{16}$	− 2.3	Querc-galloyl-hex	+
3.241	199.0596	$C_9H_{10}O_5$	− 2.5	Syringic acid	+
3.302	303.0495	$C_{15}H_{10}O_7$	− 3.3	Quercetin	+
	449.1074	$C_{21}H_{20}O_{11}$	− 2.2	Kaemp-hex	
4.129	287.0546	$C_{15}H_{10}O_6$	− 3.5	Kaempferol	+

Hi – Hibiscetin; Myr – Myricetin, Querc – Quercetin, Kaemp – Kaempferol, Hex – Hexosides, Pent-Pentosides

2565, Lonza). All strains were cultured in DMEM (Dulbecco's modified Eagle medium) with 1% penicillin/streptomycin (P/S) antibiotics and supplemented with 10% FBS (fetal bovine serum). They were kept in an incubator of CO_2 at 37 °C. *In vitro* experiments using the cells were performed in triplicate.

MTT cytotoxicity and selective index

Cells were seeded in 96-well plates at a density of 5 × 103 cells per well and incubated overnight in a CO_2 (5%) at 37 °C for plate adherence. Treatments were prepared in DMSO (1%) and DMEM supplemented with 0.5% FBS. After 24 hours, cells were treated with extracts at concentrations of 0, 5, 15, 30 and 40 µg/mL and fractions of 0, 5, 10, 15, 20, 30 and 35 µg/mL concentrations for 24 and 72 hours. The cell viability was quantified using MTT colorimetric reagent (3- [4,5-Dimethylthiazol-2-yl] − 2,5-diphenyltetrazolium bromite; Invitrogen – M6494)), and absorbance was measured using an Elisa reader, at a wavelength of 570 nm, after incubating the cells with MTT for 3 hours.

From the value obtained from the IC50, the selectivity index (SI) was calculated. The calculation was performed from the formula SI = IC50 non-tumor cells/IC50 tumor cells [36].

Wound healing cell migration

The wound healing assay evaluated the inhibitory potential of cell mobility of the extracts. The GAMG and U251 tumor cells were seeded in DMEM supplemented with 10% FBS in 24-well plates at the density of 5×10^5 cells/well. The cells were incubated overnight at CO_2 and 37 °C. Thus, two wounds were made in each well using a p200 µL tip. The wounds were washed with PBS1X to remove nonadherent cells, and soon after, treatments were added at IC50 concentration diluted in DMEM supplemented with 2% FBS. The images were obtained immediately after and subsequently at 24, 48 and 72 hours using Zen Lite 2.1 software (400× magnification). Also, cell morphology was qualitatively analyzed at 400× magnification [38].

Morphological detection of apoptosis

For the qualitative analysis of apoptosis, GAMG and U251 were seeded in a 96-well plate (75×10^3 cells/well) and incubated (24 h). Afterward, cells were exposed to IC50 value (72 h) for 24 h. The treatment-free culture was used as negative control, and cells were detached and collected at the end of each incubation time. Finally, cells were washed with PBS and incubated with a 1 : 1 ratio of 10 µL acridine orange (0.01 mg/mL) and 10 µL propidium iodide (0.01 mg/mL). Cells were viewed immediately under a fluorescent microscope vert. A1. Ten images were obtained at 200× magnification with a filter range of 450–490 nm [14]. The cells emitting a green color with intact membranes and nuclei were counted as viable cells. Cells that emitted a green color with distinct features such as membrane disruption, apoptotic bodies and chromatin condensation were counted as apoptotic. Meanwhile, red-fluorescent cells with loss of membrane integrity were assigned as necrotic. Cells were quantified using Zen software (Zeiss).

Zymography

The proteolytic enzyme activity of pro-MMP-2 was measured by gelatin zymography. The gelatinolytic activity of MMPs was investigated by zymogram. MMP-2 (10 ng/µL – REF: ab81550) and MMP-9 (10 ng/mL – REF. Ab82955) samples and treatments (IC50) were used [10]. The samples were subjected to electrophoresis through a 7% Zymogram Ready Gel (Bio-Rad Laboratories). After electrophoresis, the gel was incubated twice in 2.5% TritonX-100 for 60 min at room temperature and, then, incubated at 37 °C for 18 h in an activation buffer (10 mM Tris-HCl buffer (pH 8.0) containing 5 mM (Tris-CaCl2). Gels were stained (0.25% Comassie blue G-250, 30% ethanol, 10% acetic acid) for 1 h and destained (30% ethanol, 10% acetic acid) for 2 h. Results of the mean ± standard deviation of inhibition were converted into percentages and normalized in the presence of controls using Excel 2010 software.

Cell adhesion assay

The wells of the 96-well plate were coated with 100 µL of Matrigel diluted with 10 µg/mL BSA (1 : 10 PBS1X) and incubated in a CO_2 oven at 37 °C. Afterward, excess liquid was removed and 100 µL BSA solution (0.1%) was added to each well of the plate and again incubated for 2 hours under the same conditions. Finally, the solution was removed, the wells were washed with PBS, and GAMG and U251 (6×10^3 cells/well) were seeded in DMEM (FBS free) with the treatments IC50. The plate with the cells was incubated for 2 hours in CO_2 at 37 °C and, then, fixed with 10% trichloroacetic acid (1 hour). Finally, they were stained with violet crystal, and 100 µL of Tris-5 mM was added to the wells for a spectrophotometer reading (540 nm). Absorbance values were converted to percentage mean ± standard deviation of cell viability and normalized in the presence of the DMSO vehicle using Excel 2010 software [39].

Western blotting

Cells were cultured (7×10^5 cells/well) in DMEM (10% FBS and 1% P/S) for 24 hours. After that, they were replaced by DMEM (0.5% FBS and 1% P/S) for 24 hours. Then, the cells were treated with the IC50 of the compound for 24 hours. The harvested cells were prepared using lysis buffer (NaF, $Na3VO_3$, PiroNa, Leu, APRO, DTT, EDTA and PMSF) at 4 °C and were collected by centrifugation. Concentrations of proteins were determined by the Bradford assay (Bio-Rad, Hercules, CA) [40]. Identical amounts of proteins (20 µg) were separated by SDS-PAGE (sodium dodecyl sulfate–polyacrylamide gel electrophoresis) (concentration gels 10% and another 15%), Precision Plus Protein molecular weight (PM) standard (Bio-rad) was used as PM control. The proteins were transferred to nitrocellulose membranes (Amersham Biosciences) using the semi-dry transfer equipment (Amersham) for 4 hours at 140 V. The membrane was blocked using 5% non-fat dry milk diluted in TBST (Tris-buffered saline and Tween 20) for 1 h at room temperature and then incubated at 4 °C overnight with the specific primary antibodies (**Table 1 S**, Supplementary material). Subsequently, membranes were incubated with their respective peroxidase-conjugated secondary antibodies (anti-mouse or anti-rabbit) and were developed with enhanced chemiluminescence solution (0.1 M Tris (pH 8.5), 0.25 M luminol (Sigma-Aldrich) and 0.1 M coumaric acid (Sigma-Aldrich)). The protein expression was determined by densitometric analysis and normalized to the corresponding loading controls. Densitometry quantification was performed by ImageJ (NIH) software [41].

Chicken chorioallantoic membrane assay

CAM assay was used to assess in vivo tumor proliferation and angiogenesis. Fertilized chicken eggs (Gallus gallus) were incubated for three days at 37 °C and 70% humidity. CAM assay was used to assess in vivo tumor proliferation and angiogenesis. Fertilized chicken eggs (Gallus gallus) were incubated for three days at 37 °C and 70% humidity. Then, an opening of 1 mm in diameter was performed using sterile forceps and scissors. On the 9th day, 2×10^6 tumor cells resuspended in 20 µL of matrigel were placed in the CAM. The images of the tumors were obtained using a stereomicroscope (MOTIC 580–5.0MP) after the treatments (20 µL topically in the tumor mass) on the 14th day and the 17th day. Measuring the tumor on the 17th and subtracting from the tumor measurement on the 14th, we estimated the effect of the treatment on tumoral growth [42]. Euthanasia was performed by freezing using a − 80 °C freezer for 10 minutes [43]. CAMs were

removed and histologically analyzed by staining hematoxylin and eosin. The images were obtained at 200× magnification and the area of the tumor perimeter and quantified blood vessels with ZEN software. The Ethics Committee of the Federal University of São João Del Rei provided ethical approval under protocol number 039/2017 (December 11th, 2017). All applicable international, national and institutional guidelines for the care and use of animals were followed.

Hen's egg test – chorioallantoic membrane (het-cam) test method

The eggs were incubated for 10 days in a digital automatic brooder at 37 °C and 60 % humidity. After this incubation period, the shell and its membrane around the inner tube was removed, exposing the chorioallantoic membrane. Then, treatments (300 µL) were applied. The negative control and positive control used were 0.9 % NaCl and 1 % SDS, respectively. Images were obtained at times 0, 20, 120 and 300 seconds using the MOTIC stereomicroscope (Moticam 580–5.0MP). The chorioallantoic membrane was examined and the observed physiological reactions were graded according to their time of onset [42].

Characterization by mass spectrometry (esi-ms) and uhplc-esi-qtof

The ultra-performance liquid chromatography was performed using the UHPLC System (Agilent Technologies). An ACQUITY BEH C18 (130 Å, 1.7 µm, 2.1 × 0.4 id × 100 mm) column (Waters) at 30 °C was employed to perform the separation. The ethyl acetate fraction was diluted in 200 mL of ethanol 70 % (v/v) and additionally diluted 1 : 10 with EtOH 70 %. The fractions 01ID-F2 and 01IID-F4 were diluted in 200 mL of ethanol 70 % (v/v), and only fraction 01ID-F4 was additionally diluted 1 : 10 with EtOH 70 %. The injection volume was 1 µL. The mobile phases consisted of solvent A (0.1 % formic acid in water) and solvent B (0.1 % formic acid in acetonitrile), and the gradient elution conditions were 0–0.75 min, 1 % B; 0.75–6.0 min, 1–99 % B; 6.0–8.0 min, 99 % B; 8.0–9.0 min, 99–1 % B; 9.0–10.0 min, 1 % B, with a flow rate of 0.4 mL/min and gradient with linear changes (min/% B): 0/1, 0.75/1, 6.0/99, 8/99, 9/1, 1. The mass spectrometer was operated using an electrospray ionization source in positive and negative ion modes (one mode for run). The MS parameters were set as capillary voltage 3.00 kV, nozzle voltage 1.00 kV, drying gas N_2 temperature 350 °C, flow rate 10 L/min, nebulizer pressure 35 psi, sheath gas temperature 300 °C, sheath gas flow 10 L/min and scan range 100–1700 at a scan rate of 3.00 spectra/s.

Statistical analysis

The results obtained were analyzed using GraphPad Prisms software version 5.01 (La Jolla). The significance in all statistical analyses was considered as $p < 0.05$. Data are represented as the mean ± SD and values with different superscripts indicating statistically significant differences ($^{***}p < 0.001$; $^{**}p < 0.01$ and $^{*}p < 0.05$). Nonlinear regression was used to calculate the IC50. The tests involving comparisons were made with simple comparisons between the different conditions studied using analysis of variance followed by Tukey's post test.

Supporting Information

The effects used in the Western blotting assay and their concentrations are described in the supplemental material.

Contributors' Statement

RIMAR: conceived and designed the analysis, reviewed and edited the manuscript and acquired funding; AGSO: data collection, performed the experiments; analysis and interpretation of the data, drafting the manuscript; M. A. R., L. S. A., A. T. M. C., P. S.: data collection, analysis and interpretation of the data. R. C. R.C; H. B. S.; R. G. T., P. S.; E. W.; B. K.; R. M. R.: critical revision of the manuscript and edited the manuscript, also contributed to data analysis tools.

Funding

The authors are grateful for the research support provided by the Fundação de Amparo à Pesquisa do Estado de Minas Gerais (FAPEMIG – PPM-00229-16 and APQ-00068-18) and Coordenação de Aperfeiçoamento de Pessoal de Nível Superior (CAPES – Finance Code 001). This research was also supported by FINEP (MCTI/FINEP/MS/SCTIE/DECIT-01/2013, FPXII-BIOPLAT). Furthermore, we thank all other parties who made this study possible.

Conflict of Interest

The authors declare that they have no conflicts of interest.

References

[1] Lapointe S, Perry A, Butowski NA. Primary brain tumors in adults. The Lancet 2018; 392: 432–446

[2] Grochans S, Cybulska AM, Simińska D, Korbecki J, Kojder K, Chlubek D, Baranowska-Bosiacka I. Epidemiology of glioblastoma multiforme–Literature review. Cancers (Basel) 2022; 14: 2412

[3] Ravi VM, Will P, Kueckelhaus J, Sun N, Joseph K, Salié H, Heiland DH. Spatially resolved multi-omics deciphers bidirectional tumor-host interdependence in glioblastoma. Cancer Cell 2022; 40(6): 639–655

[4] Alifieris C, Trafalis D. T Glioblastoma multiforme: Pathogenesis and treatment. Pharmacol Ther 2015; 152: 63–82

[5] Gupta T, Talukdar R, Kannan S, Dasgupta A, Chatterjee A, Patil V. Efficacy and safety of extended adjuvant temozolomide compared to standard adjuvant temozolomide in glioblastoma: Updated systematic review and meta-analysis. Neurooncol Pract 2022; 9: 354–363

[6] Park MN, Song HS, Kim M, Lee MJ, Cho W, Lee HJ, Kim B. Review of natural product-derived compounds as potent antiglioblastoma drugs. Biomed Res Int 2017; 2017: 8139848

[7] Newman DJ, Cragg GM. Natural products as sources of new drugs from 1981 to 2014. J Nat Prod 2016; 79: 629–661

[8] Calixto JB. The role of natural products in modern drug discovery. An Acad Bras Cienc 2019; 91: (Suppl 3)

[9] Silva-Oliveira RJ, Lopes GF, Camargos LF, Ribeiro AM, Santos FV, Severino RP, Severino VG, Terezan AP, Thomé RG, Santos HB, Reis RM, Ribeiro RI. Tapirira guianensis Aubl. Extracts inhibit proliferation and migration of oral cancer cells lines. Int J Mol Sci 2016; 17(11): 1839

[10] Longatti TR, Cenzi G, Lima LARS, Oliveira RJS, Oliveira VN, Da Silva SL, Ribeiro RIMA. Inhibition of gelatinases by vegetable extracts of the species Tapirira guianensis (Stick Pigeon). British Journal of Pharmaceutical Research 2011; 1: 133

[11] Stockhammer F. Treatment of glioblastoma in elderly patients. CNS Oncol 2014; 3: 159–167

[12] Tan AC, Ashley DM, López GY, Malinzak M, Friedman HS, Khasraw M. Management of glioblastoma: State of the art and future directions. CA Cancer J Clin 2020; 70(4): 299–312

[13] Silva AG, Lopes CFB, Júnior CGC, Thomé RG, Dos Santos HB, Reis R, Ribeiro RIMA. MWIN55, 212-2 induces caspase-independent apoptosis on human glioblastoma cells by regulating HSP70, p53 and Cathepsin D. Toxicol In Vitro 2019; 57: 233–243

[14] Indrayanto G, Putra GS, Suhud F. Validation of in-vitro bioassay methods: Application in herbal drug research. Profiles Drug Subst Excip Relat Methodol 2021; 46: 273–307

[15] He Y, Zhao C, Liu Y, He Z, Zhang Z, Gao Y, Jiang J. RETRACTED ARTICLE: MiR-124 functions as a tumor suppressor via targeting hCLOCK1 in glioblastoma. Mol Neurobiol 2017; 54: 2375

[16] Abba M, Patil N, Allgayer H. MicroRNAs in the regulation of MMPs and metastasis. Cancers (Basel) 2014; 6(2): 625–645

[17] Memmel S, Sukhorukov VL, Höring M, Westerling K, Fiedler V, Katzer A, Krohne G, Flentje M, Djuzenova CS. Cell surface area and membrane folding in glioblastoma cell lines differing in PTEN and p53 status. PLoS One 2014; 9: e87052

[18] Xie Q, Mittal S, Berens ME. Targeting adaptive glioblastoma: An overview of proliferation and invasion. Neuro Oncol 2014; 16(12): 1575–1584

[19] Rachlin K, Moore DH, Yount G. Infrasound sensitizes human glioblastoma cells to cisplatin-induced apoptosis. Integr Cancer Ther 2013; 12(6): 517–527

[20] Pezzani R, Salehi B, Vitalini S, Iriti M, Zuñiga F, A., Sharifi-Rad J, Martins N. Synergistic effects of plant derivatives and conventional chemotherapeutic agents: An update on the cancer perspective. Medicina (Kaunas) 2019; 55(4): 110

[21] Pistritto G, Trisciuoglio D, Ceci C, Garufi A, D'Orazi G. Apoptosis as anticancer mechanism: Function and dysfunction of its modulators and targeted therapeutic strategies. Aging 2016; 8: 603–619

[22] Abotaleb M, Samuel SM, Varghese E, Varghese S, Kubatka P, Liskova A, Büsselberg D. Flavonoids in cancer and apoptosis. Cancers (Basel) 2019; 1(1): 28

[23] Tsai YJ, Chen BH. Preparation of catechin extracts and nanoemulsions from green tea leaf waste and their inhibition effect on prostate cancer cell PC-3. Int J Nanomedicine 2016; 11: 1907–1926

[24] Wang LX, Shi YL, Zhang LJ, Wang KR, Xiang LP, Cai ZY, Zheng XQ. Inhibitory effects of (−)-Epigallocatechin-3-gallate on Esophageal cancer. Molecules 2019; 24(5): 954

[25] Kohn EC, Liotta LA. Molecular insights into cancer invasion: Strategies for prevention and intervention. Cancer Res 1995; 55(9): 1856–1862

[26] Liu Y, Tang ZG, Yang JQ, Zhou Y, Meng LH, Wang H, Li CL. Low concentration of quercetin antagonizes the invasion and angiogenesis of human glioblastoma U251 cells. Onco Targets Ther 2017; 10: 4023–4028

[27] Santos BL, Oliveira MN, Coelho PL, Pitanga BP, Da Silva AB, Adelita T, Costa SL. Flavonoids suppress human glioblastoma cell growth by inhibiting cell metabolism, migration, and by regulating extracellular matrix proteins and metalloproteinases expression. Chem Biol Interact 2015; 242: 123–137

[28] Han L, Zhang HW, Zhou WP, Chen GM, Guo KJ. The effects of genistein on transforming growth factor-β1-induced invasion and metastasis in human pancreatic cancer cell line Panc-1 in vitro. Chin Med J (Engl) 2012; 125(11): 2032–2040

[29] Yang CS, Wang H. Cancer preventive activities of tea catechins. Molecules 2016; 21(11): 2032–2040

[30] Busch M, Philippeit C, Weise A, Dünker N. Re-characterization of established human retinoblastoma cell lines. Histochem Cell Biol 2015; 143(3): 325–338

[31] Dünker N, Jendrossek V. Implementation of the Chick Chorioallantoic Membrane (CAM) model in radiation biology and experimental radiation oncology research. Cancers (Basel) 2019; 11(10): 1499

[32] Zhao B, Hu M. Gallic acid reduces cell viability, proliferation, invasion and angiogenesis in human cervical cancer cells. Oncol Lett 2013; 6(6): 1749–1755

[33] McLaughlin N, Annabi B, Bouzeghrane M, Temme A, Bahary JP, Moumdjian R, Béliveau R. The Survivin-mediated radioresistant phenotype of glioblastoma is regulated by RhoA and inhibited by the green tea polyphenol (−)- epigallocatechin-3-gallate. Brain Res 2006; 1071(1): 1–9

[34] Mukherjee S, Baidoo JN, Sampat S, Mancuso A, David L, Cohen LS, Banerjee P. Liposomal tricurin, a synergistic combination of curcumin, epicatechin gallate and resveratrol, repolarizes tumor-associated microglia/macrophages, and eliminates glioblastoma (GBM) and GBM stem cells. Molecules 2018; 23(1): 201

[35] Taibi A, Bardet MS, Durand Fontanier S, Deluche E, Fredon F, Christou N, Mathonnet M. Managing chemotherapy extravasation in totally implantable central venous access: Use of subcutaneous wash-out technique. J Vasc Access 2020; 21(5): 723–773

[36] Eichenbaum G, Zhou J, De Smedt A, De Jonghe S, Looszova A, Arien T, Goethen FV, Vervoort L, Skukla U, Lammens L. Methods to evaluate and improve the injection site tolerability of intravenous formulations prior to first-in-human testing. J Pharmacol Toxicol Methods 2013; 68(3): 394–406

[37] Pluschnig U, Haslik W, Bartsch R, Mader RM. Extravasation emergencies: State-of-the-art management and progress in clinical research. Memo 2016; 9(4): 226–230

[38] Wang X, Decker CC, Zechner L, Krstin S, Wink M. *In vitro* wound healing of tumor cells: Inhibition of cell migration by selected cytotoxic alkaloids. BMC Pharmacol Toxicol 2019; 20: 4

[39] Salo T, Sutinen M, Hoque Apu E, Sundquist E, Cervigne NK, de Oliveira CE, Akram SU, Ohlmeier S, Suomi F, Eklund L, Juusela P, Åström P, Bitu CC, Santala M, Savolainen K, Korvala K, Leme AFP, Coletta RD. A novel human leiomyoma tissue derived matrix for cell culture studies. BMC Cancer 2015; 15: 981

[40] Bradford M. A rapid and sensitive method for the quantitation of microgram quantities of protein utilizing the principle of protein-dye binding. Anal Biochem 1976; 72: 248–254

[41] Pereira DG, Salgado MA, Rocha SC, Santos HL, Villar JA, Contreras RG, Fontes CFL, Barbosa LA, Cortes VF. Involvement of Src signaling in the synergistic effect between cisplatin and digoxin on cancer cell viability. J Cell Biochem 2018; 119(4): 3352–3362

[42] Silva AG, Silva VAO, Oliveira RJS, Rezende AR, Chagas RCR, Lúcia LPS, Romão W, Santos HB, Thomé RG, Reis RM, Ribeiro RIMA. Matteucinol, isolated from Miconia chamissois, induces apoptosis in human glioblastoma lines via the intrinsic pathway and inhibits angiogenesis and tumor growth in vivo. Invest New Drugs 2020; 38(4):1044–1055

[43] Underwood W. AVMA Guidelines for the Euthanasia of Animals: 2013 Edition. Schaumburg, IL: American Veterinary Medical Association; 2013